The Journal of Experimental Biology 202, 3239–3254 (1999)
Printed in Great Britain © The Company of Biologists Limited 1999
JEB2444

LOADING CONDITIONS AND CORTICAL BONE CONSTRUCTION OF AN ARTIODACTYL CALCANEUS

STEVEN C. SU[1], JOHN G. SKEDROS[1], KENT N. BACHUS[2] AND ROY D. BLOEBAUM[1,*]

[1]*Bone and Joint Research Laboratory, Department of Veteran's Affairs Medical Center, 500 Foothill Boulevard, Salt Lake City, UT 84148, USA* and [2]*Orthopedic Bioengineering Research Laboratory, University of Utah, Salt Lake City, UT 84112, USA*

*Author for correspondence (e-mail: roy.bloebaum@hsc.utah.edu)

Accepted 6 September; published on WWW 28 October 1999

Summary

Customary nonuniform distributions of physiological bone strains are thought to evoke heterogeneous material adaptation in diaphyseal cortices of some limb bones. Recent studies of artiodactyl calcanei have suggested that the regional prevalence of specific mechanical strain features such as mode and magnitude correlate with specific variations in cortical bone ultrastructure, microstructure and mineralization. These data are also consistent with predictions of current algorithms of mechanically induced bone adaptation. However, detailed characterization of the customary functional strain environment of these bones is needed to understand better the mechanisms of these adaptations.

An *in vitro* loading method and rosette strain gauges were used to record principal strains, maximum shear strains and principal strain angles at multiple locations on ten calcanei of adult male mule deer (*Odocoileus hemionus hemionus*). Each hind limb was fixed in an apparatus to mimic the mid-support phase of the gait and loaded *via* the Achilles tendon over a broad range of functional loads (0 to 2943 N). Strains were recorded on the craniolateral, craniomedial, caudal, medial and lateral cortices at mid-diaphysis. Loading variations included the progressive elimination of the ligament and tendon along the caudal calcaneus.

The results showed that the cranial cortex experiences longitudinal compressive strains that are nearly equal to the principal minimum strains and that the caudal cortex receives longitudinal tensile strains that are nearly equal to the principal maximum strains. With a 981 N load, the mean principal compressive strain on the cranial cortex was −636±344 με (mean ± S.D., *N*=9) and the mean principal tensile strain on the caudal cortex was 1112±68 με (*N*=9). In contrast to the cranial and caudal cortices, principal strains in the medial and lateral cortices displayed relatively large deviations from the longitudinal axis (medial, 24° cranial; lateral, 27° caudal). Although shear strains predominated at all gauge sites, variations in maximum shear strains showed no apparent regional pattern or consistent regional predominance. The plantar ligament and tendon of the superficial digital flexor muscle were shown to have important load-sharing functions.

These results demonstrate that the functionally loaded artiodactyl calcaneus generally behaves like a cantilevered beam with longitudinal compression and tension strains predominating in opposing cranial and caudal cortices, respectively. Differences in osteon remodeling rates, osteon morphology and mineral content reported previously between the cranial and caudal cortices correlate, in part, with the magnitudes of the principal compressive and tensile strains, respectively. However, material differences that distinguish the medial and lateral cortices from the cranial and caudal cortices could not be primarily attributed to locally increased shear strains as previously suggested. Variations in osteon and/or collagen fiber orientation may correlate more strongly with principal strain direction.

Key words: artiodactyl calcaneus, bone strain, cortical bone morphology, bone adaptation, bone remodelling, mechanostat theory.

Introduction

Using artiodactyl (sheep, deer, elk) and perissodactyl (horse) calcanei from skeletally mature animals, recent studies (Skedros, 1994; Skedros et al., 1994a,b, 1997, 1998) have provided evidence consistent with the hypothesis that cortical bone adapts in response to specific features of its habitual strain environment, namely strain magnitude and mode (i.e. tension, compression, shear) (Martin and Burr, 1989, pp. 156–163; Riggs et al., 1993; Mason et al., 1995; Skedros et al., 1996). These studies documented marked differences in cortical thickness, mineral content (% ash), microstructure (e.g. secondary osteon population density) and ultrastructure (e.g. preferred collagen fiber orientation) between cortices that were considered to

experience primarily compressive (cranial cortex) or tensile (caudal cortex) strains. For example, the ‘compression’ cortices of these ‘tension/compression’ bones have increased mineral content and osteon population density and more oblique-to-transverse collagen fibers than the opposing ‘tension’ cortices (Skedros, 1994; Skedros et al., 1998).

These findings extend and support previous studies that have reported some similar regional differences (preferred collagen fiber orientation, osteon orientation and/or osteon population density) in diaphyseal cortices of other bones that experience customary, directionally consistent bending (e.g. human proximal femur, horse radius, horse third metacarpal, sheep radius, turkey ulna) (Portigliatti Barbos et al., 1984; Martin and Burr, 1989, pp. 69–70, 157–158; Riggs et al., 1993; Skedros, 1994; Hert et al., 1994; Mason et al., 1995; Martin et al., 1996; Petrtyl et al., 1996; Skedros et al., 1994a,b, 1995, 1996, 1997, 1998). These recent investigators have proposed several interrelated causal/mechanistic explanations for these differences, including: (1) customary nonuniform distributions of strain modes and/or directions are associated with strain gradients that mediate the production of regional differences in preferred collagen fiber orientation and osteon orientation; (2) regional differences in strains, when of sufficient magnitude, affect threshold-related mechanisms that mediate the production of regional differences in secondary osteon population density, remodeling rates and mineral content; and (3) customary regional prevalence of specific strain modes may cause regional disparities in ultrastructural/microstructural damage, which subsequently results in heterogeneity in cortical material construction.

Recent studies have also shown that calcanei of selected artiodactyl and perissodactyl species have medial and lateral cortices that (compared with their ‘tension’ and ‘compression’ cortices) typically have fewer, and more oblong, secondary osteons and intermediate mineral content (Skedros et al., 1997). These differences have been attributed to shear strains that are thought to be customarily elevated in the medial and lateral cortices (Skedros et al., 1997). In contrast to the medial, lateral and cranial cortices, the caudal calcaneal cortex exhibits a relatively low mineral content, an increased porosity and an increased prevalence of relatively large, irregularly shaped newly forming secondary osteons (Skedros et al., 1994a,b, 1997). These caudal cortex features may reflect an increased bone renewal rate in a region where peak strain magnitudes are insufficient for maintaining tissue mass (Skedros et al., 1997). Such osteonal remodeling was noted to be consistent with increased remodeling activity below a low-strain remodeling threshold described in detail by Frost’s mechanostat hypothesis of mechanically mediated bone adaptation (Frost, 1990a,b, 1997a,b; Skedros et al., 1994a,b, 1997). Consequently, it has been suggested that the caudal cortex consistently experiences functional strain magnitudes well below those in the neighboring medial, lateral and cranial cortices (Skedros et al., 1997). In turn, it has been hypothesized (Skedros et al., 1997) that these three cortical regions habitually experience higher strains that are within a range where remodeling and modeling events are relatively quiescent (Frost, 1990a,b; Burr, 1992; Huiskes et al., 1992; Carter et al., 1996).

Interpretations of the functional relevance of, and the mechanisms that mediate, these heterogeneities in material

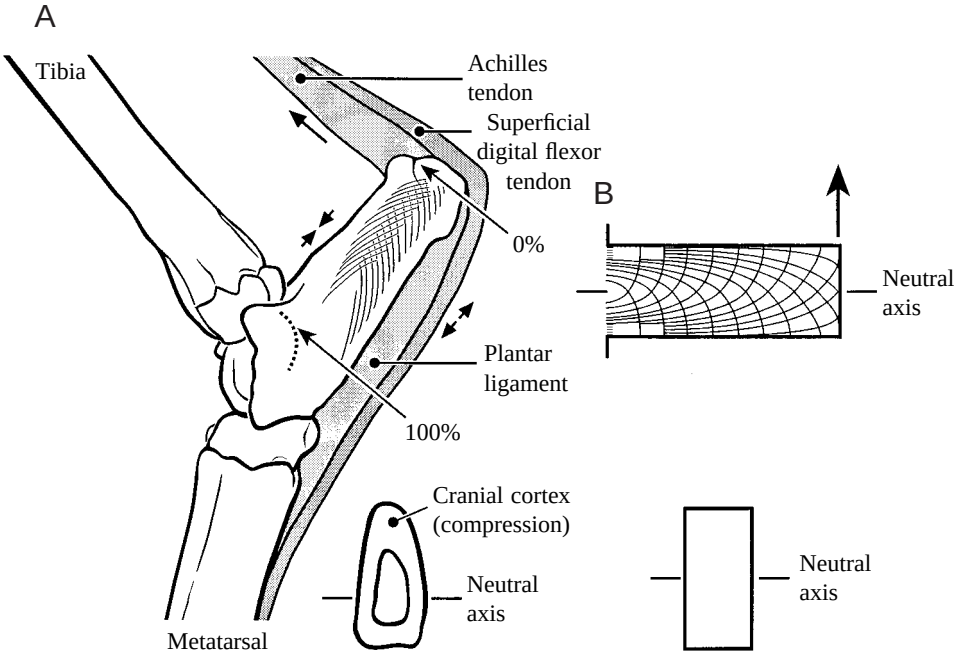

Fig. 1. (A) Lateral-to-medial view of the ankle joint of a skeletally mature mule deer. Percentage diaphysis length locations are defined by the 0 % arrow at the distal calcaneal tuber and the 100 % arrow at the inflection of the dotted contour line formed by the proximal calcaneus articular surface. The trabecular bone patterns are stylized on the calcaneus and are based on a lateral-to-medial roentgenogram. The arrow adjacent to the Achilles tendon indicates the direction of force imparted to the calcaneus by the Achilles tendon and m. superficial digital flexor tendon during the middle of the support phase, placing the cranial cortex in compression (converging arrows). The lower drawing represents a transverse section of the calcaneus at 50 % diaphysis length and indicates a possible location of a theoretical neutral axis based on ideal beam behavior. (B) Diagram of a rectangular prismatic cantilevered beam loaded at its free end as indicated by the vertical arrow. Principal strain trajectories are drawn on the lateral view of the beam (redrawn from Currey, 1984, p. 140). Trajectories at the base of cantilever have been omitted for clarity. As a first approximation, functional end-loading of the calcaneus presumably produces strain patterns similar to those of the illustrated cantilevered beam. The neutral axis is shown on both the lateral (upper) and transverse (lower) views of the beam.

construction were based on the premise that the diaphyses of these calcanei experience a customary nonuniform strain distribution similar to that of a short cantilevered beam loaded at its free end (Fig. 1B). Hence, longitudinal compressive strains dominate in the cranial cortex, longitudinal tensile strains dominate in the caudal cortex and maximum shear strains dominate along the neutral axis of bending. Although previous *in vivo* strain gauge analyses of sheep calcaneal diaphyses show some strain features of cantilevered bending (Lanyon, 1973, 1974; Skerry and Lanyon, 1995), the development of this analogy was limited since these previous studies used only one rosette strain gauge on any given bone. Hence, the conception of artiodactyl and perissodactyl calcanei as relatively simple cantilevered beams has not been rigorously established. Basic strain data are needed to examine these bones more critically for mechanically mediated bone adaptation.

The first hypothesis tested in the present study is that physiological end-loading *via* the Achilles tendon of the mule deer calcaneus produces longitudinal compression strains in the cranial diaphyseal cortex and longitudinal tensile strains in the caudal diaphyseal cortex. It has been suggested that strain mode and magnitude differences between these opposing cortices may strongly influence their conspicuous morphological differences. The second hypothesis tested is that, during physiological loading, the highest shear strains occur along the medial and lateral cortices of the calcaneus. Local shear strain variations may help to explain regional variations in some material features of cortical construction. The final hypothesis tested is that the plantar ligament (which is adherent to the calcaneal caudal cortex) and superficial digital flexor tendon (Fig. 1A) share tensile loads with the caudal cortex, keeping this region habitually in a low-strain environment (low or 'trivial' loading zone) (Fig. 2) (Skedros et al., 1997).

To test these hypotheses, an *in vitro* loading method and multiple rosette strain gauges were used to measure principal tensile and compressive strain magnitudes and directions and maximum shear strains at the same locations where regional ultrastructure, microstructure and mineral content variations have been reported in previous studies (Fig. 3). To test the final hypothesis, strains at these locations were also measured with and without transection of the plantar ligament and superficial digital flexor tendon. If these structures have important load-sharing functions, then strains should increase after their transection.

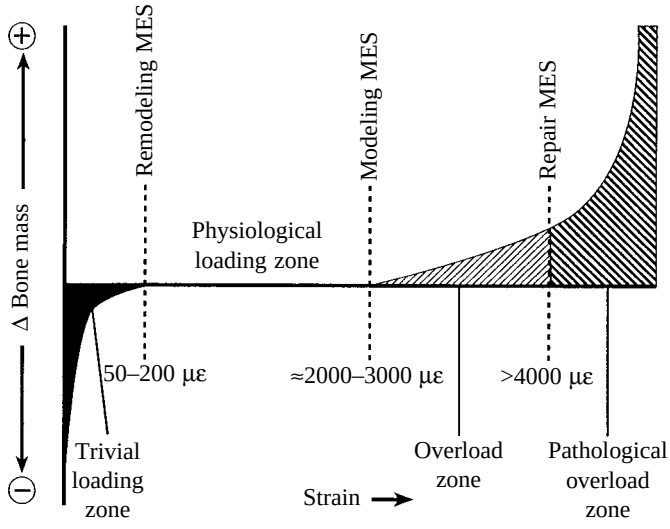

Fig. 2. Graphical illustration of the four mechanical usage 'windows' of Frost's mechanostat theory (after Fig. 4 in Burr, 1992). Each loading zone is defined by strain magnitude thresholds (horizontal axis) which predict bone remodeling and/or modeling activities resulting in an increase or decrease in bone mass (Δ bone mass, vertical axis). Below the remodeling minimum effective strain (MES or trivial loading zone), strains are low and bone remodeling is activated to decrease bone mass. This MES is analogous to the 'lazy' zone described by Carter et al. (1996) and the 'dead' zone described by Huiskes et al. (1992) (see Burr, 1992). Above the remodeling MES but below the modeling MES (the physiological loading zone), remodeling activity is relatively repressed and there is no net change in bone mass. At higher strains just above the modeling MES, lamellar bone is formed, causing an increase in bone mass. When strains are greater than the repair MES (pathological overload zone), new woven bone is added to bone surfaces and probably represents a repair reaction.

Materials and methods

In this study, principal maximum strains are referred to as principal tensile strains and principal minimum strains are referred to as principal compressive strains. For statistical analyses, compressive strain data were analyzed as absolute values. Strain gauge locations, shown in Fig. 3, are expressed in the text using both the anatomical location and the gauge number in parentheses [e.g. medial (6)].

Hind limb preparation

One hind limb from 10 skeletally mature, wild, male mule deer (*Odocoileus hemionus hemionus*) was frozen upon retrieval and thawed before experimentation. The maturity of each calcaneus was confirmed by a fused distal growth plate (Purdue, 1983). The dressed mass of the animals averaged 82 kg (range 68–90 kg). After cutting each limb at mid tibia, the tibial diaphysis was inserted into a tube of polyvinyl chloride and fixed with epoxy resin (Supermend, Titan Corp., Lynnwood, WA, USA). The longitudinal axis of the tube and tibia were collinear. The potted tibia was then secured into position using an apparatus (Fig. 4) constructed of steel tubing with a square cross section (3.18 cm×3.18 cm). The acute angle subtended by the longitudinal axis of the principal metatarsal and horizontal ground was fixed at 60 °, and the obtuse angle subtended by the long axis of the metatarsal and tibia was fixed at 120 °. This limb position represents the middle of the support phase in galloping roe deer (*Capreolus capreolus*) as shown by cinematographic frames from Gambaryan (1974). At this instant, the ground-reaction force of trotting sheep and dogs is

maximal and acts almost entirely in the vertical direction (the horizontal component is less than 3% of the vertical component) (Jayes and Alexander, 1978). Within a similar range of gaits and speeds, it is assumed that the mule deer hind limb will exhibit ground-loading conditions that are comparable with those reported in sheep and dogs during mid-support phase. This assumption is supported by force-plate data for goats (Pandy et al., 1988) and by studies showing similar vertical and horizontal ground-reaction forces in a wide variety of animals including rams (*Ovis musimon*), dogs (*Canis familiaris*) and hares (*Pedetes cafer*) (Cavagna et al., 1977). These studies showed that the vertical ground-reaction force approaches a maximum while the horizontal component approaches zero during the mid-support phase in a controlled gait cycle. Strains on sheep calcanei are also maximal at this limb position during walking (Lanyon, 1973). In general, the moment around the ankle joint of quadrupeds is maximal near the mid-support phase (Biewener, 1989). These data formed the basis for selecting the limb position used in the present study.

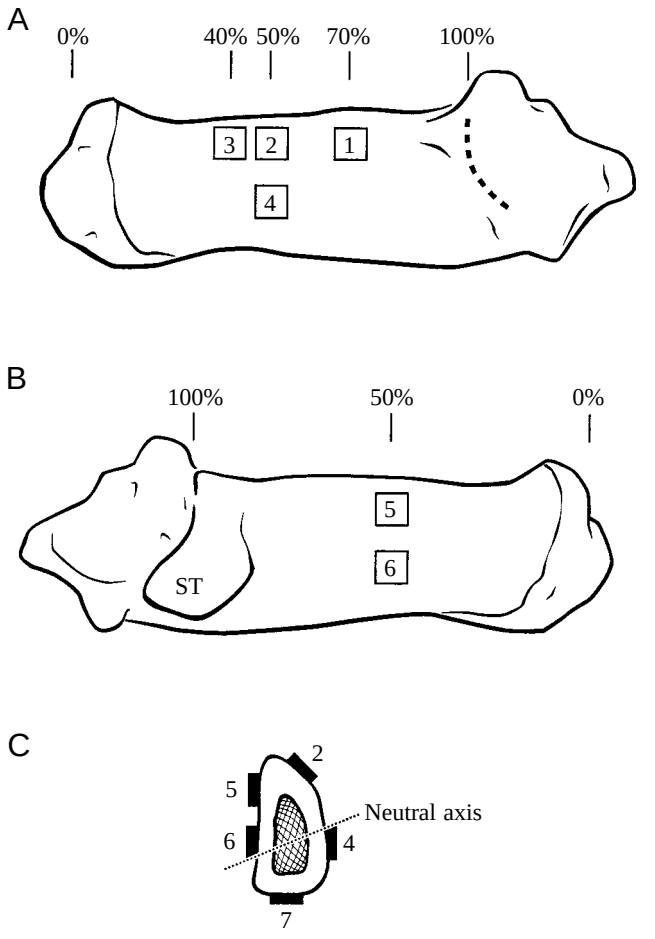

Fig. 3. Strain gauge locations on the calcaneal diaphysis. (A) Lateral view of the calcaneus. Gauges 1, 2 and 3 are located on the craniolateral cortex, and gauge 4 is located on the lateral cortex. The broken line indicates the projected contour of the proximal articular surface. (B) Medial view of the calcaneus. Gauge 5 is located on the craniomedial cortex, and gauge 6 is located on the medial cortex. ST, sustentaculum talus. In A and B, numbers above the diagrams indicate percentage diaphyseal length. (C) Transverse view at 50% diaphyseal length. Gauge 7 is located on the caudal cortex. The dotted line in C represents a possible location of the neutral axis, based on the present study's experimental strain gauge data.

The Achilles and m. superficial digital flexor (SDF) tendons were sewn together to a strip of aramide fabric that provided a loop for attaching a piece of aramide cord (Gemini, Black Diamond Ltd, Salt Lake City, UT, USA). The cord was passed through the two pulleys of the loading apparatus and connected to a screw-driven universal testing machine (model 1125, Instron Inc., Canton, MA, USA) (Fig. 4). Locomotor strains were simulated by pulling simultaneously on the Achilles and SDF tendons in a direction parallel to the longitudinal axis of the tibia (Fig. 4). Since the tendons, the aramide cord and their attachment could stretch during loading, the crosshead travel was manually controlled by the operator. This ensured that the required force was applied in each loading cycle (described further below). Applied loads were measured using a 500 kg rated load cell (model A217-17A, Instron Inc., Canton MA, USA). Reaction forces at the hoof were simultaneously monitored with another load cell (MC3A, AMTI Corp., Newton, MA, USA) which recorded forces in the vertical and anterior-to-posterior directions.

Pilot studies showed that reaction forces at the hoof were not predominantly in the vertical direction, which this study had intended to simulate, but had a notable horizontal component. In addition, upon loading of the Achilles tendon, the hoof slid 2.5–6.0 cm on the force plate. This was caused by interphalangeal laxity, resulting in excessive dorsiflexion at the hoof. To restrict this excessive motion, it would have been necessary to apply a substantial load to the deep digital flexor tendon. This motion was minimized by fitting small triangular metal wedges behind the hoof and attaching the wedge to the platform with screws. A supplementary fixator plate was also fastened across the interphalangeal and metatarsal–phalangeal joints. This fixator consisted of an aluminum bar and two brackets rigidly attached to the metatarsal bone and proximal phalanges (Fig. 4). Experimental support for fixing the hoof to the load cell was found in a previous study in which both *in vitro* and *in vivo* strains were measured on potoroo (a small marsupial) calcanei (Biewener et al., 1996). The *in vitro* data, which were obtained after rigidly fixing the potoroo foot, did not differ significantly from the *in vivo* data (unpublished results and details of fixation were provided by A. A. Biewener).

Strain gauge measurement

Using a scalpel, strain gauge sites were manually scraped clean of adherent tissue and then degreased using ether; this process was repeated twice to ensure a clean bonding surface. Rosette strain gauges (WA-060-120-WR, Measurements Group Inc., Raleigh, NC, USA) were then bonded to the bone using cyanoacrylate adhesive (M-bond 200, Measurements

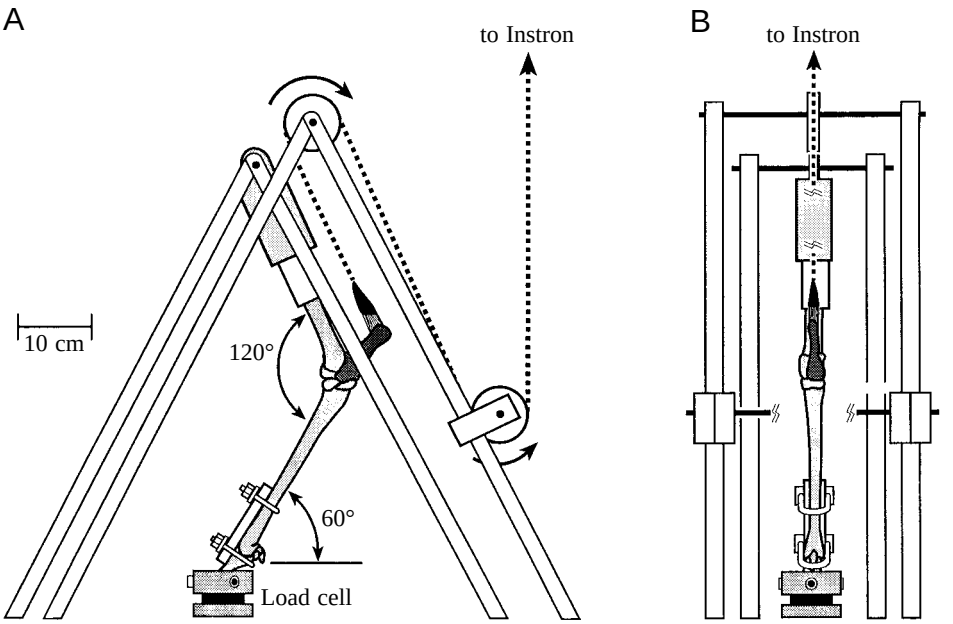

Fig. 4. Apparatus used to hold the mule deer hind limb during testing. (A) Lateral-to-medial view; (B) posterior-to-anterior view. The broken lines in A and B represent the aramide cord that was used to transfer forces from the Instron machine to the calcaneus. Crossbars used to enhance rigidity of the apparatus are omitted for clarity.

Group Inc., Raleigh, NC, USA) at the locations shown in Fig. 3. In each case, one strain gauge of the rosette was aligned parallel with the longitudinal axis of the calcaneus. The longitudinal axis was defined as the chord connecting the 0 % and 100 % diaphyseal length locations in accordance with previously described methods (Skedros et al., 1994a) (Fig. 1). Each strain gauge was wired to a Wheatstone bridge circuit and supplied with a constant current of 13.75 mA (AIFP Instrumentation Amplifier, Microstrain Inc., Burlington, VT, USA). This device also amplified the strain gauge signal, which was collected and stored using a 486 computer through an A/D board (AT-MIO-64E-3, National Instruments Inc., Austin, TX, USA). Data were sampled at 30 Hz using a data-acquisition software package (Measure, National Instruments Inc., Austin, TX, USA). Principal tensile strains, principal compressive strains, maximum shear strains and principal strain angles were calculated using standard engineering formulae (Dally and Riley, 1991).

Strains were measured at applied loads (force applied, F_a) of 491 N, 981 N, 1962 N and 2943 N, which correspond to vertical ground-reaction forces of approximately 0.3, 0.5, 1.0 and 1.5 times body weight, respectively. These percentage of body weight values were calculated using the same method of static analysis used by Dimery and Alexander (1985) to estimate the forces acting on the donkey calcaneus that counteract the maximum vertical ground-reaction force incurred during a running gait. Vertical ground-reaction force in a trotting sheep approximates 0.5 times body weight (Jayes and Alexander, 1978) and is estimated to be 0.65–1.25 times body weight in running horses (Dimery and Alexander, 1985; Biewener et al., 1988). Thus, a vertical ground-reaction force of 1.5 times body weight produced by the greatest load applied in the present study (2943 N) simulates a gait more aggressive than typical trotting. The range of loads used in the present study ensured sampling from a range of possible load magnitudes, presumably corresponding to various locomotor activities.

To minimize adhesive degradation, testing was completed on the same day that gauges were bonded to bone. Testing was performed at room temperature (20–22 °C), and soft tissues were moistened with physiological saline. Up to four test trials were performed on each limb. Each trial consisted of three cycles, and in each cycle the calcaneus was loaded from 0 N to the specified peak load and back to 0 N. To provide reliable results, the crosshead speed of the Instron was 500 mm s^{-1} and the loading duration of each cycle was approximately 10 s. This produced strain rates of approximately 265 $\mu\varepsilon\ s^{-1}$. Although strain rates of this magnitude occur on artiodactyl limb diaphyses during physiological locomotion (Lanyon and Baggot, 1976; Goodship et al., 1979; O'Connor et al., 1982), this rate is considerably slower than those measured on calcanei of walking sheep (approximately 2500 $\mu\varepsilon\ s^{-1}$) (Lanyon, 1973). However, recent experimental data demonstrate that the elastic modulus of compact bone exhibits minimal variation across a broad range of physiological strain rates (100–160×10^3 $\mu\varepsilon\ s^{-1}$) (Currey, 1988; Evans et al., 1992). Since stress is linearly related to strain by Hooke's law, peak bone strains measured at these rates would not be expected to vary greatly across a broad range of strain magnitudes. Although bone is not a purely Hookean material, cortical bone closely resembles one, where strain increases in direct proportion to the applied stress (Currey, 1984; Martin and Burr, 1989). These facts support the use of the strain rate used in this study for the limited comparisons with strain data reported in sheep calcanei.

Trial 1: baseline strains

In trial one, seven limbs were used to measure strains at locations 1–6 (Fig. 3). Subsequently, three additional animals

were included, but strains were only recorded at locations 2, 4 and 6. Strains were initially measured at more locations because they coincide with regions where ultrastructure, microstructure and mineral content have been analyzed (Skedros et al., 1994a,b, 1997, 1998). Applied loads were from 0 N to a peak load of 2943 N.

Trial 2: plantar ligament separated

The same ten specimens used in trial 1 were used in trial 2. In trial 2, a scalpel was used to separate the plantar ligament from the caudal cortex between 20 % and 80 % of diaphyseal length (Skedros et al., 1994a) (Fig. 1). Although separated from its cortex, the plantar ligament remained in continuity to maintain its longitudinal load-carrying capacity. The entire caudal aspect of the calcaneal diaphysis forms a firmly adherent attachment for the plantar ligament (Skedros et al., 1994a), and separating this ligament from the bone was necessary to attach a strain gauge to the caudal cortex at 50 % diaphysis length. Strains were measured at locations 2, 4, 5, 6 and 7 (Fig. 3). Applied loads were the same as in trial 1, 0 N to a peak load of 2943 N.

Trial 3: plantar ligament separated and transected

Trial 3 used eight of the ten specimens used in trial 2. One omitted specimen sustained an epiphyseal separation (as described below) and the other specimen could not be tested within the same day that the gauges were bonded. In the remaining eight specimens, the plantar ligament was completely transected at 70 % of calcaneal diaphysis length; hence, it could no longer carry loads along the caudal aspect of the calcaneus. The SDF tendon remained intact. Applied loads were from 0 to 1962 N, and bone strains were recorded at locations 2, 4, 6 and 7. The applied load was reduced from the original peak load of 2943 N used in trials 1 and 2 because an epiphyseal separation occurred at the distal epiphysis in one specimen at 2943 N, rendering the limb useless for further testing. This occurred in a trial where both the plantar ligament and the SDF tendon were cut. Although cutting the SDF tendon is a procedure of trial 4 and not of trial 3, it was decided that the 2943 N load should also be reduced to 1962 N in trial 3 to prevent possible damage to other limbs. This reduction was not expected to alter the recorded strain patterns because of the nearly identical strain profiles produced by these two loads. Furthermore, because the strain patterns of the failed specimen in trials 1 and 2 closely resembled those in other bones, the initial data from the failed specimen were not discarded.

Trial 4: plantar ligament separated and transected and SDF tendon transected

Using the same eight specimens of trial 3, the SDF tendon was completely severed at 70 % diaphysis length (Fig. 1), in addition to the previous separation and transection of the plantar ligament. As in trial 3, the strains were measured at locations 2, 4, 6 and 7 with loads from 0 to 1962 N. In this trial, loads applied to the calcaneus were transmitted solely by the Achilles tendon.

Statistical analyses

Comparisons of principal compressive and tensile strain magnitudes measured at the same gauge were evaluated using a paired *t*-test. One-way analysis of variance (ANOVA) was used to evaluate multiple comparisons of maximum shear strains and principal strain angles; Fisher's least significant difference test was used to evaluate pairwise comparisons between gauge sites. In cases where maximum shear strain and principal angle data sets were not normally distributed, the Kruskal–Wallis test was used with a Kruskal–Wallis multiple-comparison *Z*-value to detect pairwise differences. Comparisons among principal compressive and tensile strains, maximum shear strains and principal strain angles between trial 1 and trials 2, 3 and 4 were evaluated using paired *t*-tests for the same gauge location. In a few instances, there was not a complete pair of data to perform the paired *t*-test. This was due to a poorly bonded gauge or accidental cutting of the strain gauge terminal lead wires. A poorly bonded gauge was identified by voltage signals that drifted continuously. When either of these two cases occurred, the unpaired data were not included when computing the percentage difference. In all comparisons, absolute values of principal compressive strains were used. A P value greater than 0.01 but less than 0.05 was considered to indicate a statistical trend, and $P<0.01$ was considered to be statistically significant.

Results

Fig. 5 shows the waveforms of principal compressive and tensile strains and of maximum shear strains during three loading cycles in trial 1 at the craniolateral (2) gauge (animal C117). These waveforms are representative of the sample and were nearly identical for most trials and locations. Notable exceptions (e.g. in trials 3 and 4) are described below. As load was applied to each calcaneus, the principal tensile and compressive strains increased in magnitude and reached a maximum concurrent with the peak applied load. With few exceptions, the same topographic patterns and relative regional differences in strain were found at each applied load.

Table 1 contains means and standard deviations of strain data at 491 N at 50 % gauge locations [craniolateral (2), craniomedial (5), medial (6), lateral (4) and caudal (7)]. Fig. 6 presents histograms of 981 N, 1962 N and 2943 N load data for all trials. Data from craniolateral (1) and craniolateral (3) gauges are not reported in detail because they were similar to those for the nearby craniolateral (2) gauge. Means were computed using strain data from the first half of the loading cycle; for example, the data points for the first peak (tensile strains) or trough (compression strains) in Fig. 5. Strains in trial 1 are considered as 'baseline' strains because strains at some locations differ notably between trials 1 and 2, and because there was no alteration to the plantar ligament or SDF tendon. Relative differences between other trials are shown in Table 1 and Fig. 6.

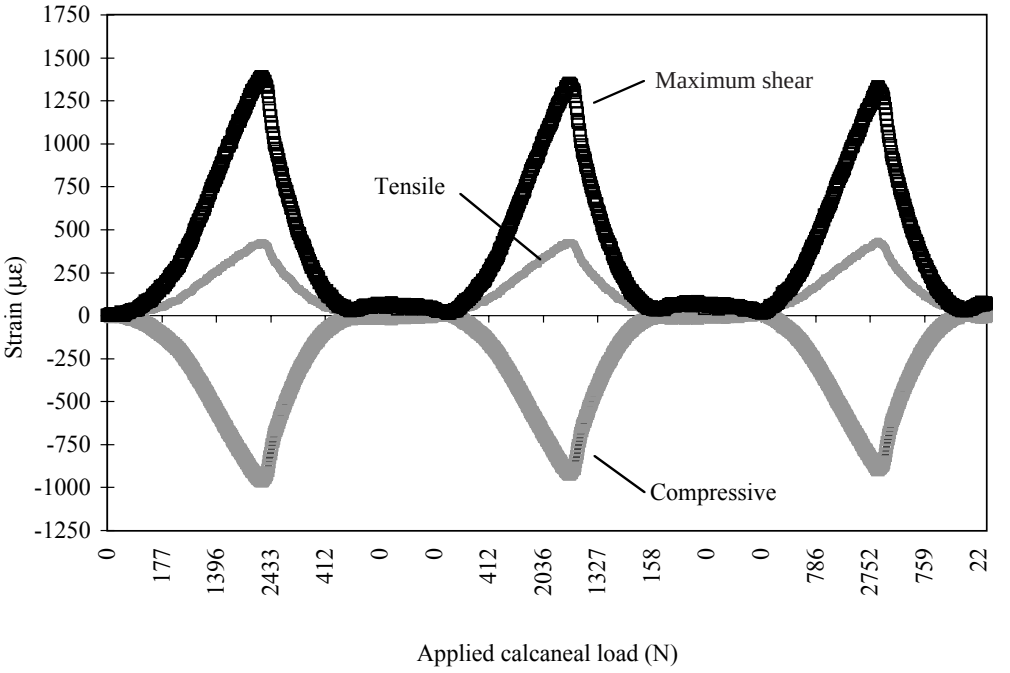

Fig. 5. Principal compressive strain, principal tensile strain and maximum shear strain waveforms recorded in trial 1 at the 50 % craniolateral gauge (gauge 2) (animal C117).

Table 1. *Strain variables at 50 % length and 491 N applied load*

Gauge site	Trial	*N*	Principal tensile strain (με)	Principal compressive strain (με)	Maximum shear strain (με)	Principal angle (degrees)	Principal strain ratio	Dominant strain mode
Craniolateral	1	9	170.9±52.4	–348.4±177.0	519.3±225.8	–84.8±5.2	2.0	c
(2)	2	9	155.1±60.9	–292.9±153.6	448.0±210.9	–85.4±5.6	1.9	c
	3	8	185.4±57.8	–357.4±161.7	542.8±216.7	–88.3±6.1	1.9	c
	4	7	218.5±96.7	–374.1±249.7	592.5±345.2	–86.1±8.5	1.7	c
Craniomedial	1	6	183.8±67.9	–323.7±158.0	507.5±219.1	–80.4±7.2	1.8	c
(5)	2	5	181.0±41.6	–309.8±136.7	490.7±175.5	–81.3±8.3	1.7	c
	3	NA	NA	NA	NA	NA	NA	NA
	4	NA	NA	NA	NA	NA	NA	NA
Medial	1	10	192.0±60.2	–389.3±155.9	581.3±212.9	–66.0±6.4	2.0	c
(6)	2	9	199.3±47.5	–372.5±159.1	571.8±200.7	–64.8±7.2	1.9	c
	3	8	197.2±49.2	–277.3±143.9	474.5±177.0	–60.6±7.9	1.4	c
	4	7	245.0±96.8	–111.0±91.3	356.0±139.6	–33.4±19.1	0.5	t
Lateral	1	10	348.1±132.1	–135.6±29.2	483.7±142.1	–27.6±26.3	0.4	t
(4)	2	10	330.7±128.1	–159.3±52.3	489.9±150.7	–28.1±25.5	0.5	t
	3	8	373.6±130.6	–165.2±87.9	538.8±208.6	–39.7±15.6	0.4	t
	4	8	511.1±178.7	–311.1±75.4	822.2±236.6	–31.0±25.8	0.6	t
Caudal	1	NA	NA	NA	NA	NA	NA	NA
(7)	2	7	590.6±93.4	–195.2±65.8	785.8±140.5	4.6±5.6	0.3	t
	3	7	803.0±192.6	–317.3±131.3	1120.3±302.6	0.2±4.0	0.4	t
	4	5	1218.2±288.3	–459.1±118.1	1677.3±401.3	–2.1±3.8	0.4	t

Values are means ± S.D.; NA, not applicable.
The principal strain ratio is the absolute value of (principal compressive strain/principal tensile strain).
c, compression; t, tension.

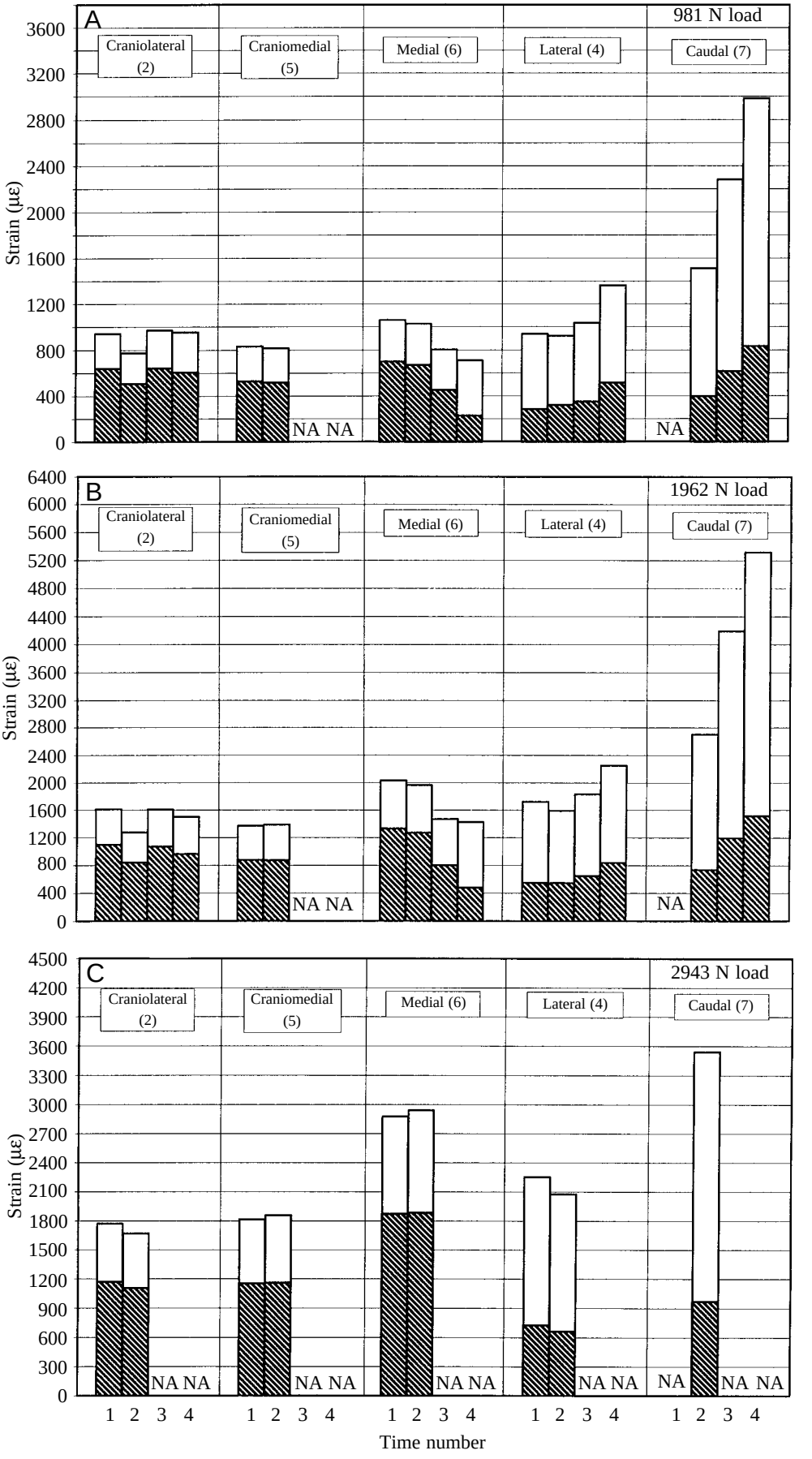

Fig. 6. Strain parameters at 50 % length and loads of 981 N (A), 1962 N (B) and 2943 N (C) in trials 1–4. The heights of the hatched bars represent principal compressive strains (absolute value), and the heights of the open bars represent principal tensile strains. The total height of the hatched and open bars represents the maximum shear strain. NA, not applicable.

Table 2. *P values from paired* t*-tests of principal compressive strain* versus *principal tensile strain from trial 1 except for the caudal gauge, which was taken from trial 2*

Applied load (N)	Craniolateral (1)		Craniolateral (2)		Craniolateral (3)		Lateral (4)		Craniomedial (5)		Medial (6)		Caudal (7)	
	Ratio	*P* value	Ratio	*P* value	Ratio	*P* value	Ratio	*P* value	Ratio	*P* value	Ratio	*P* value	Ratio	*P* value
491	1.87	0.008	2.0	0.002	2.4	0.004	2.6*	0.0005	1.8	0.01	2.0	<0.0001	3.0*	<0.0001
981	1.8	0.01	2.1	0.002	2.3	0.0004	2.3*	0.0006	1.8	0.02	2	0.0001	2.8*	<0.0001
1962	1.7	0.03	2.1	0.003	2.2	0.002	2.1*	0.0003	1.75	0.03	1.9	0.0002	2.7*	<0.0001
2943	1.7	0.03	1.9	0.001	2.3	0.003	2.1*	0.0005	1.72	0.04	1.87	0.0003	2.6*	0.0002

Ratio, strain ratio (principal compressive strain/principal tensile strain) (gauges 1, 2, 3, 5 and 6) or (principal tensile strain/principal compressive strain) (gauges 4 and 7).

*Tension greater than compression.

Trial 1

Principal compressive and tensile strains

At all loads, mean principal compressive strains in trial 1 were at least 1.7 times greater (P<0.04) than principal tensile strains at the craniolateral (1, 2, 3), craniomedial (5) and medial (6) gauges (Tables 1, 2; Fig. 6). For example, with a 981 N load, the craniolateral (2) gauge showed that the mean principal compressive strain exceeded the mean tensile strain by 2.1-fold (−636.4±343.7 με *versus* 306.4±95.8 με) (Fig. 6A). Thus, the compressive strains were the major principal strain component of the craniolateral (1, 2, 3), craniomedial (5) and medial (6) gauges. In contrast, at each load, lateral (4) principal tensile strains were at least 2.1 times greater (P<0.001) than corresponding principal compressive strains (Table 2). For example, at 981 N load, the mean lateral (4) principal tensile strain was 654.9±250.8 με and the mean principal compressive strain was −283.9±45.5 με. Thus, tension was the major principal strain component at the lateral (4) gauge.

Maximum shear strains

The mean maximum shear strains at the craniolateral (2), craniomedial (5), medial (6) and lateral (4) gauges did not differ significantly (P>0.10) at F_a=491 N and 981 N (Table 1; Fig. 6). At higher applied loads (1962 N, 2943 N), there were few significant differences between cortices. Among the various applied loads, the maximum shear strains at each of the medial (6) and lateral (4) gauges did not exhibit consistent differences compared with the craniomedial (5) and craniolateral (2) gauges (e.g. compare Fig. 6A,C).

Principal angle

Principal strain angles were measured with reference to the longitudinal axis of the calcaneus (Fig. 7). The mean principal angles at the craniolateral (2) gauge were −85.0±4.9° (mean ± S.D.) (F_a=1962 N) and −87.7±9.5° (F_a=2943 N), those at the craniomedial (5) gauge were −79.5±5.6° (F_a=1962 N) and −78.2±5.2° (F_a=2943 N), those at the medial (6) gauge were −65.6±8.6° (F_a=1962 N) and −64.3±8.9° (F_a=2943 N), and those at the lateral (4) gauge were −30.0±6.5° (F_a=1962 N) and −29.4±6.6° (F_a=2943 N). In most paired comparisons (e.g. craniolateral *versus* lateral, craniolateral *versus* medial, etc.), principal angles at the 50 % locations were statistically different. These data demonstrate that these locations experience significantly different principal strain orientations. The only exception was the craniolateral (2) *versus* craniomedial (5) comparison, which was not statistically different at F_a=1962 N.

Principal strain comparisons of trial 1 with trials 2, 3 and 4: medial (6) and lateral (4) gauges

The purposes of trials 2, 3 and 4 were to determine the degree of load-sharing of the plantar ligament and SDF tendon.

Trial 1 versus *trial 2*

In trial 2, the plantar ligament was separated from the caudal cortex. This separation was expected to alter strains across the bone section. However, the mean medial (6) principal compressive strains generally exhibited rather small decreases between trials 1 and 2 (e.g. –4.3 %, P=0.003) (Table 1; Fig. 6). Minor differences in principal compressive strains between trials 1 and 2 also occurred at the lateral (4) gauge, but these differences were not statistically significant (P>0.10).

Mean medial (6) and lateral (4) principal tensile strains were not statistically different between trials 1 and 2 (P>0.10; F_a=491–1962 N) (Table 1; Fig. 6).

The relatively small differences between trials 1 and 2 suggest that separation of the plantar ligament did not greatly affect the strain environment at the medial (6) and lateral (4) gauges.

Trial 1 versus *trial 3*

In trial 3 the plantar ligament, which had been separated from the caudal cortex (trial 2), was completely transected. The mean medial (6) principal compressive strains decreased considerably in magnitude and were statistically different compared with values for trial 1 (–29 %, P=0.002, F_a=491 N; –35 %, P=0.002, F_a=981 N; –40 %, P<0.001, F_a=1962 N) (Table 1; Fig. 6). In contrast, the mean medial (6) principal tensile strains of trial 3 did not differ statistically compared with values for trial 1 (P>0.42; F_a=491 N, 981 N, 1962 N). Thus, separation and transection of the plantar ligament decreased principal compressive strain magnitudes on the medial cortex.

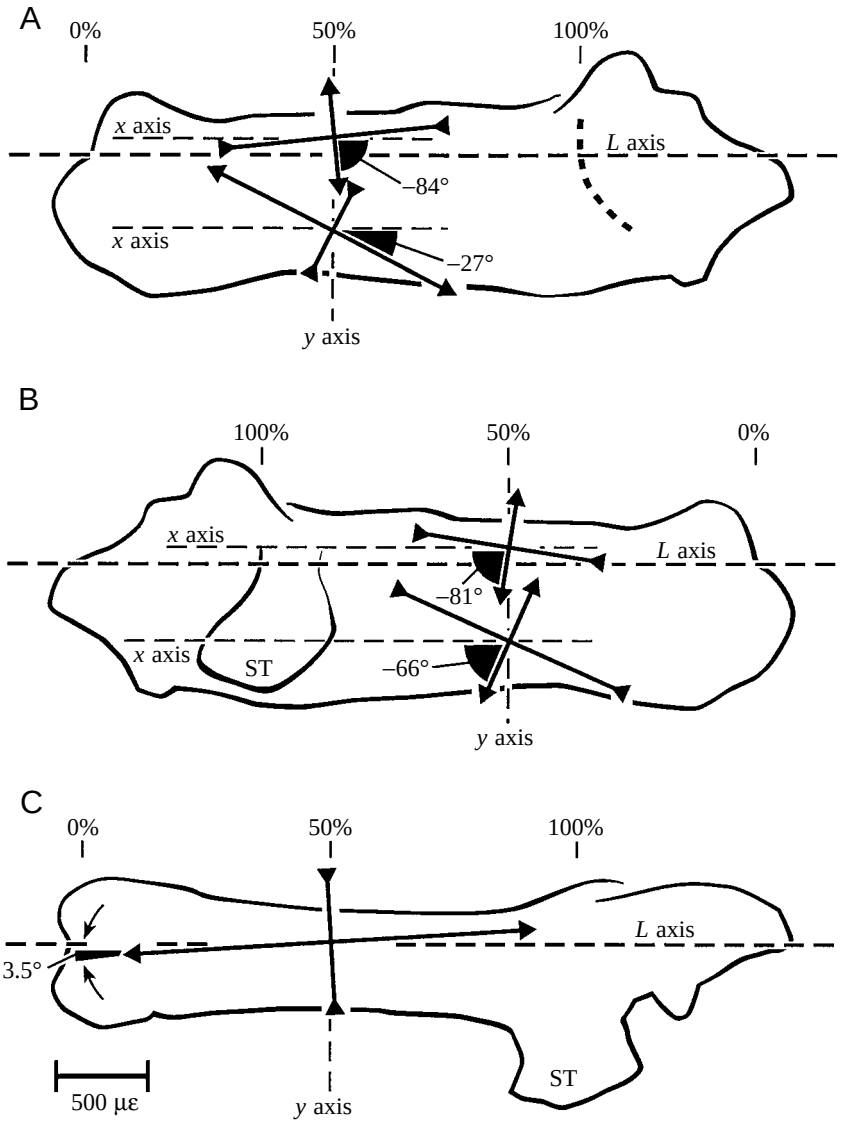

Fig. 7. Orientation of principal strains with reference to the longitudinal axis (L axis) of the calcaneus. Converging arrows indicate principal compressive strain; diverging arrows indicate principal tensile strain. The scale bar indicates principal strain magnitudes. (A) Lateral view showing principal angles at the craniolateral (2) (top) and lateral (4) (bottom) gauges; (B) medial view showing the principal angles at the craniomedial (5) (top) and medial (6) (bottom) gauges; (C) caudal view showing principal angle at the caudal (7) gauge. Data in A and B are from trial 1 and 981 N load. Data in C are from trial 2 (plantar ligament separated from caudal cortex) and 981 N load. ST, sustentaculum talus.

In most cases, there were no statistical differences in the mean lateral (4) principal compressive strains between trials 1 and 3 (P=0.12, F_a=491 N; P=0.11, F_a=981 N). Thus, separation and transection of the plantar ligament did not consistently alter the principal strains on the lateral cortex.

Trial 1 versus *trial 4*

Transection of the SDF tendon in trial 4 had an even larger effect on strains at both the medial (6) and lateral (4) gauges. Between trials 1 and 4, mean medial (6) principal compressive strains decreased by 64 % and 71 % at loads of 491 N and 1962 N, respectively (P<0.001) (Table 1; Fig. 6). In contrast, the mean medial (6) principal tensile strains typically did not differ statistically between trials 1 and 4 at 491 and 981 N loads (P=0.33 and P=0.08, respectively). Therefore, transection of the SDF tendon (trial 4) consistently decreased the principal compressive strains on the medial cortex.

Between trials 1 and 4, the mean lateral (4) principal compressive strains increased by 129 % and 52 % (P<0.01) at loads of 491 N and 1962 N, respectively. Mean lateral (4) principal tensile strains also increased markedly between trials 1 and 4 at loads of 491 N, 981 N and 1962 N (47 %, P=0.003; 29 %, P=0.01; 31 %, P=0.09, respectively) (Table 1; Fig. 6). In general, transection of the SDF tendon in trial 4 increased the principal compressive and tensile strains on the lateral cortex.

Comparing the results of trials 2, 3 and 4 with those of trial 1 demonstrates that the principal strains of the medial and lateral cortices were not greatly affected (<5 %) by the separation of the plantar ligament (trial 2) but were increasingly affected by the sequential transection of the plantar ligament (trial 3) and the SDF tendon (trial 4) (Fig. 6).

Principal strain comparisons among all trials; craniolateral (2) gauge

In contrast to the results reported for the medial and lateral gauges (described above), plantar ligament separation (trial 2) tended to decrease principal compressive strains at the craniolateral (2) gauge (e.g. −16 % and −23 % at F_a=491 N

and 1962 N, respectively; P=0.2). However, subsequent transection of the plantar ligament (trial 3) and SDF tendon (trial 4) resulted in only relatively minor changes in the craniolateral (2) principal tensile and compressive strain magnitudes (Table 1; Fig. 6). Compared with changes at the medial and lateral gauges, minor variations in cranial principal stains suggest that transection-related changes in neutral axis location most notably affect strains at the medial, lateral and caudal gauges. Compared with the cranial cortex, these cortices are narrower and less mineralized (Skedros et al., 1994a, 1997).

All trials: shear data

Maximum shear strains did not show clear patterns of regional variation at all loads. For example, although the highest shear strains were expected to occur in the medial and lateral cortices (i.e. along the neutral axis), this only occurred at F_a=1962 N and 2943 N (Fig. 6B,C). From trials 1–4, the changes in shear strain magnitudes that occurred at the medial, lateral and cranial gauges generally paralleled the changes in principal strains at the same gauge locations (Fig. 6). This is because maximum shear strain was calculated directly from the principal strains.

Principal strain comparisons of trial 2 with trials 3 and 4; caudal (7) gauge

Recall that a caudal gauge was not used in trial 1 because placement of a gauge on the caudal cortex required separation of the plantar ligament. This was accomplished in trial 2.

Trial 2 versus *trial 3*

Differences in caudal (7) principal compressive strains between trials 2 and 3 were not statistically significant (P>0.09) (Table 1; Fig. 6). In contrast, the mean caudal (7) principal tensile strains increased by 36 % and 77 % (P<0.02; F_a=491 N and 1962 N, respectively) between trials 2 and 3, respectively. Therefore, transection of the plantar ligament (trial 3) tended to increase principal tensile strains on the caudal cortex.

Trial 2 versus *trial 4*

At the caudal (7) gauge, principal compressive strain magnitudes increased by 135 % and 107 % (P<0.02; F_a=491 N and 1962 N, respectively) between trials 2 and 4 (Table 1; Fig. 6). Similarly, mean caudal (7) principal tensile strains increased by 106 % and 92 % (P<0.02; F_a=491 N and 1962 N, respectively). Therefore, the additional transection of the SDF tendon markedly increased the principal compressive and tensile strain magnitudes on the caudal cortex.

Discussion

As noted by Hallgrimsson and Swartz (1995), in the explanation of morphological variations in relation to a proposed functional context, one must entertain three alternative hypotheses: (1) that the morphological feature in question is an adaptation to a hypothesized functional context; (2) that the hypothesized functional context is incorrect or incomplete and that the morphological feature(s) in question is adapted to some other or more complete functional context; and (3) that the morphological feature in question does not meet the predictions of the functional context for reasons contingent to functional consideration such as developmental bias and constraint. Obviously these hypotheses are not mutually exclusive alternatives. In all cases, all three will be true to varying degrees. The identification of a functional context from which to frame an adaptationist hypothesis is inevitably a subjective abstraction imposed on a more complex reality. Although rejecting the second hypothesis is never possible, the more one knows of the functional context, the less emphasis one can place on it. Thus, the better the functional context is known, the more one's test of an adaptive hypothesis becomes a test of functional determinism as an explanation of morphological variation (Hallgrimsson and Swartz, 1995).

The hypotheses considered in the present study, including those dealing with relationships between specific strain features and local material construction, have the advantage of being framed against a relatively simple and well-understood functional context. The unidirectional, cantilevered-beam-like loading of the sheep calcaneus has been demonstrated by *in vivo* strain analysis, and the predictability of loading in bending is firmly based in behavioral observations and experiments. The results of the present study reveal that functional loading of the mule deer calcaneus similarly produces a strain environment that is generally consistent with the bending of a cantilevered beam. We previously hypothesized that specific features of the non-uniform strain distribution produced by this simple loading environment were causally related to the topographically heterogeneous material construction of the cortical bone. This hypothesis seems tenable in several contexts, including (1) the proposition that regional disparities in mechanical properties of bone in tension, compression and shear would provide sufficient 'forces' to drive this morphological adaptation, (2) previous studies suggesting that bone tissue may exhibit the accumulated effects of its strain history (Lanyon and Baggott, 1976; Carter et al., 1980; Carter, 1984, 1987; Burr, 1992; Riggs et al., 1993; Levenston et al., 1994; van der Meulen et al., 1996; Reilly et al., 1997; Skedros et al., 1996), and (3) the proposition that bone tissue may embody a 'memory' of important aspects of past and/or current loading conditions (Skerry et al., 1990; Brand, 1992; Riggs et al., 1993; Levenston et al., 1994; Skedros et al., 1994a,b, 1996, 1998; Mason et al., 1995; Takano et al., 1999).

Although data reported in the present study are not sufficient to test this hypothesis and its corollaries adequately, they challenge some of our previous simplistic functional explanations. For example, deviations from the predicted simple loading environment are especially notable in the caudal ('low-strain') cortex and in the medial and lateral ('shear') cortices. Alternative functional explanations for the regional variations in the construction of these cortices are considered below.

Cranial and caudal cortices

The cranial strains (gauges 1, 2, 3 and 5; Fig. 3) recorded in this study support the hypothesis (Skedros et al., 1997) that functional loading of the mule deer calcaneus produces near-longitudinal (6° off axis) principal compressive strains in the cranial cortex that are within a range of strains where modeling/remodeling activities are relatively quiescent (Fig. 2) (Frost, 1990a,b; Huiskes et al., 1992; Carter et al., 1996). Strains recorded from the caudal (7) gauge are consistent with the hypothesis that the caudal cortex experiences near-longitudinal (3.5° off axis) principal tensile strains. However, the present data challenge a previous hypothesis that the caudal cortex experiences relatively low strains. These strains were believed to be below a theoretical threshold of approximately 200 με where osteon remodeling is relatively active, resulting in a net loss of bone (Frost, 1997a,b) (Fig. 2). However, this threshold should still be considered provisional since its true value is not known.

The caudal cortex: a low-strain environment?

Previous suggestions that the caudal cortex customarily experiences low strain were based on data showing that this region exhibits several characteristics expected in a low-strain environment, including (1) increased population densities of newly forming secondary osteons, (2) relatively decreased mineral content, presumably as a result of reduced mean tissue age, and (3) increased porosity as a result of forming secondary osteons (Skedros et al., 1994a,b, 1995, 1997). Although it has been hypothesized that this increased remodeling activity reduces cortical bone mass in response to very low strains (below 200 με) (Skedros et al., 1994a,b, 1997), the results of the present study challenge this hypothesis.

Recall that, in trial 2, the plantar ligament was separated from the caudal cortex so that a strain gauge could be placed on the caudal surface. Subsequently, in trial 3, the separated plantar ligament was transected (the SDF tendon remained intact) and caudal strains were remeasured. Comparison of the average caudal principal tensile strains between trials 2 (591 με, separated ligament) and 3 (803 με, separated and transected ligament) showed a 36% increase (P=0.02) at F_a=491 N. Thus, the intact plantar ligament reduces caudal strains by 26% and 43% at F_a=491 N and 1962 N, respectively. Caudal tensile strains before plantar ligament separation can be calculated after assuming (1) a linear increase in caudal strains with plantar ligament separation and transection, and (2) that the increase in caudal tensile strains after plantar ligament separation is equivalent to the increase after plantar ligament transection. Consequently, the peak caudal (7) principal tensile strain magnitude before plantar ligament separation at 491 N load can be estimated to be 379 με [the value for trial 2 minus the increase in strain between trials 2 and 3; 591−212=379 με]. Similar calculations at 981 N and 1962 N loads give 562 με and 944 με, respectively. These *in vitro* data suggest that the surface of the caudal cortex typically experiences moderately elevated peak strains. It is conceivable that the apparent increased remodeling activity of the caudal cortex is mediated by regionally distinct strain characteristics that are not based on the conventional understanding of strain-magnitude thresholds (Martin and Burr, 1989, pp. 156–163; Mikic and Carter, 1995; Rubin et al., 1996).

Mechanical synergy and the 'fibro-osseous' caudal cortex

The hypothesis that the plantar ligament and SDF tendon significantly reduce bending of the calcaneal diaphysis by carrying tensile loads (Skedros et al., 1994a,b, 1997) was based on studies showing that the ligaments and tendons in sheep and deer feet serve an important role in regulating the magnitude of functional stresses imposed on the ankle region (Ker, 1981; Dimery et al., 1986). This hypothesis is supported by data from the present study showing that transection of these structures substantially increased tensile strains on the caudal cortex (approximately 97% for F_a=491 N, 981 N and 1962 N). In addition, the resulting asymmetric changes in the craniomedial, craniolateral, medial and lateral gauges reflect a change in strain distribution. Transection-related variations in strain magnitudes were most notable in the medial, lateral and caudal cortices. Compared with these regions, the compression cortex is probably less affected because it is relatively thicker and has a higher mineral content (Skedros et al., 1994a, 1997).

The enthesis formed by the plantar ligament and caudal cortex has also been described as a 'fibro-osseous' cortex, where the cooperative mechanical function of these two firmly attached components is significantly altered after ligament separation (Skedros et al., 1994a,b). As suggested by the calculations in the above discussion, caudal tensile strain magnitudes increase after ligament separation. However, the mechanical synergy implied by the concept of a 'fibro-osseous' cortex is supported more directly by quantitative data showing that plantar ligament separation tended to reduce compressive strains on the opposite cranial cortex (e.g. −16% and −23% at F_a=491 N and 1962 N, respectively) (Table 1). These data suggest that detachment of the plantar ligament shifts the neutral axis towards the cranial cortex and imply that the caudal cortex and/or the plantar ligament carry greater tensile loads. In this context, if the plantar ligament carries disproportionately greater tensile loads than the caudal cortex, then the caudal tensile surface strains estimated above (e.g. 379 με at F_a=491 N) may be too high. A device designed for measuring caudal cortical surface strains without requiring plantar ligament separation will be required to examine this possibility further.

Medial and lateral cortices, shear strain data and principal strain orientation

The results of the present study do not support the hypotheses that the medial and lateral strain environments are similar and exhibit the highest shear strains (Skedros et al., 1994a,b, 1997). Principal compressive strains predominated (compared with principal tensile strains) in the medial cortex, as in the cranial cortex. In contrast, principal tensile strains predominated (compared with principal compressive strains) in

the lateral cortex, as in the caudal cortex (Tables 1, 2). This pattern was consistent at all four applied loads. Therefore, these data contradict the claims of preferential organization of collagen fiber orientation to the simple strain mode prevailing in the cranial (compression) and caudal (tension) cortices (Skedros, 1994; Skedros et al., 1994a,b, 1997). However, this does not preclude the possibility that preferred collagen fiber and/or osteon orientations have more complex functional relationships with respect to the directions of principal and shear strain modes prevailing in each cortex.

Principal strain orientation

The inconsistent relationship between a simple, prevailing strain mode and ultrastructural/microstructural construction may be clarified, in part, by referring to principal strain angle data. At the medial and lateral gauges, principal strains were obliquely oriented with respect to the long axis of the calcaneus. In contrast, the orientations of principal strains in the cranial and caudal cortices were more closely aligned with the long axis of the bone (Fig. 7). The hypothesis that principal strain directions may influence the ultrastructural/microstructural features that distinguish the medial/lateral cortices from the cranial and caudal cortices is indirectly supported by several previous studies. It has been suggested that secondary osteon orientations in limb bone diaphyses correspond to the orientation of the dominant, local principal strain (Lanyon and Bourn, 1979; Martin and Burr, 1989, pp. 158–159, 167–173; Hert et al., 1994; Petrtyl et al., 1996). A postulated mechanism for this relationship is that osteoclast/osteoblast units detect and follow directions of maximum principal strain during osteon formation (Martin and Burr, 1989, pp. 167–173). If this were true, then the secondary osteons at the locations measured in the medial and lateral cortices would be oriented obliquely with respect to the long axis of the calcaneus. This possibility is supported by quantitative data showing that secondary osteons are typically oblong in transversely sectioned medial and lateral cortices compared with the relatively circular osteons of the nearby cranial and caudal cortices (Skedros et al., 1997). In addition, oblique osteon orientations may explain, in part, why the medial and lateral cortices have preferred collagen fiber orientations that differ notably from those of the cranial and caudal cortices (Skedros, 1994). A functional explanation for such regional osteon and/or collagen fiber orientation differences is that they reduce potentially deleterious local lamellar shear stresses within osteons and/or between osteons and the interstitial matrix (Martin and Burr, 1989, pp. 158–159).

Validity of in vitro *data (deer* versus *sheep calcanei)*

In vitro strain magnitudes measured in the present study approximate *in vivo* strains reported on calcanei of walking sheep (Lanyon, 1973, 1974) (Table 3). Additional *in vivo* sheep calcaneus strain-gauge recordings performed by Skerry and Lanyon (1995) also resemble the strain magnitudes recorded in the present study. However, it is difficult to draw direct comparisons between these previous results and the data of the present study since these previous investigators did not report the exact location of the strain gauge, except that it was placed laterally. However, the fact that peak principal strains were compressive suggests that the placement was on the craniolateral cortex. This is supported by *in vivo* data of Lanyon (1973, 1974) showing that peak principal strains on sheep calcanei during walking are typically compressive in the craniolateral cortex. Thus, the strain gauge placement in Skerry and Lanyon (1995) probably corresponds to the craniolateral (2) gauges in the present study. At this location, *in vitro* mean principal compressive strains on deer calcanei (−1096 με and −1168 με at F_a=1962 N and 2943 N, respectively) resemble *in vivo* mean principal compressive strains measured during kicking in sheep (−1147 με) (Skerry and Lanyon, 1995). Principal compressive strains of this magnitude in deer

Table 3. *Comparison of Lanyon's (1973, 1974)* in vivo *principal strain values with* in vitro *strains from the present study at comparable strain gauge sites*

Gauge site	Loading procedure	Principal tensile strain (με)	Principal compressive strain (με)	Principal angle (degrees)	Principal strain ratio
Craniolateral	*In vitro**	171	−348	−85	2.0
	*In vivo***	69	−200	−88	2.9
	In vivo‡	70	−200	–	2.9
Lateral	*In vitro**	348	−136	−28	0.4
	In vivo†	300	−204	−30	0.7

In vivo data were measured in walking sheep.

In vitro data were measured at 491 N applied load to the calcaneus, which corresponds to 0.3 times body weight at hind hoof and is also approximately equivalent in walking sheep.

*Data from the present study.

**Animal 1 of Lanyon (1974).

†Animal 8 of Lanyon (1974).

‡Animal S.53 of Lanyon (1973).

Principal strain ratio: the absolute value of (minimum principal strain/maximum principal strain).

calcanei presumably occur during some locomotor activities such as the common bounding gait known as the ‘pronk’ or ‘stott’, which is more demanding than a trot or run (Hildebrand, 1977).

Principal strains and other features of a complex strain milieu

Principal strains were analyzed in the present study since previous investigators have suggested that they are important signals in the attainment and maintenance of a bone’s morphology (Lanyon, 1974; Lanyon and Bourn, 1979; Frost, 1990a,b, 1997a,b; Pead and Lanyon, 1990; Riggs et al., 1993; Biewener and Bertram, 1994; Hert et al., 1994; Rubin and Lanyon, 1984, 1987; Skedros et al., 1994a,b, 1997; Biewener et al., 1996; Turner, 1998). However, other strain-related stimuli that exist concurrently with the principal strains and at the same gauge site may contribute to the biomechanically relevant signals that bone cells perceive either directly or indirectly (Martin and Burr, 1989; Turner et al., 1995; Rubin and McLeod, 1996; Rubin et al., 1996; Judex et al., 1997). Future investigations of bone adaptation using artiodactyl calcanei must examine these various stimuli in the context of a total daily loading history, including magnitudes of applied loads (measured herein) as well as number of cycles. Future studies must also (1) quantify energy-equivalent strain values since this measure includes the influence of shear strains (Mikic and Carter, 1995) which, in the case of the artiodactyl calcaneus, predominate at every gauge location, (2) examine causal relationships such as the influence of principal strain directions and complex strain mode environments on osteon orientation and collagen fiber orientation, and (3) better characterize and control the specific epigenetic stimuli that mediate the attainment and maintenance of the heterogeneous structural and material construction of this bone.

Concluding remarks

The results of this *in vitro* biomechanical study demonstrate that the functionally loaded mule deer calcaneus generally behaves like a cantilevered beam with longitudinal compression and tension strains predominating in opposing cranial and caudal cortices, respectively. Previous studies have shown conspicuous differences in the tissue construction between opposing ‘compression’ and ‘tension’ cortices of sheep, deer, elk and horse calcanei. Although it has been suggested that many of these differences may be related to relative differences in the regional prevalence of tension, compression and shear strain modes, data from the present study in mule deer calcanei suggest that some of these differences (e.g. osteon remodeling rates, osteon morphology and mineral content) may correlate more strongly with the magnitudes of principal compressive and tensile strains. However, material differences that distinguish the medial and lateral cortices from the cranial and caudal cortices could not be primarily attributed to locally increased shear strains as previously suggested. It is also suggested that regional variations in osteon and/or collagen fiber orientation may correlate more strongly with local principal strain direction.

But attributing specific material adaptations to specific features of a bone’s functional strain milieu belies causal/mechanistic structure–function relationships that are undoubtedly more complex, probably involving various other strain stimuli. Consequently, controlled experimental studies are needed to determine whether the regional prevalence of one or more specific strain features (e.g. strain modes, magnitudes and directions) represents a sufficient stimulus for mediating the corresponding variations in osteon construction and remodeling rates of sheep, elk, deer and horse calcanei.

Artiodactyl and perissodactyl calcanei may prove to be useful models for clarifying the mechanisms that govern a limb bone’s hierarchical trabecular and cortical construction and for extrapolating findings to the limb skeletons of humans and many other animals, since they (1) have unusual heterogeneous material characteristics within the same bone section, (2) have extensive, and regionally variable, secondary osteon remodeling activities and/or characteristics (in contrast to the rat model, for example, which does not typically exhibit secondary osteon remodeling until extremely advanced age), (3) have relatively simple patterns of trabecular architecture, (4) have relatively simple and predictable habitual loading environments and strain distributions, and (5) are amenable to analyses using multiple rosette strain gauges.

The authors thank Bettina Willie and Dr Eric Vajda for criticisms of the manuscript, Chad Marriott and Dave Schoralle for technical support and Gwenevere Shaw for clerical support. We are grateful to Drs David R. Carrier and Dennis M. Bramble for offering their expertise and advice on the biomechanics of quadrupedal locomotion. This work was supported by medical research funds from the Orthopedic Bioengineering Research Laboratory, Department of Orthopedics, University of Utah School of Medicine, Salt Lake City, Utah, USA, and the Department of Veteran’s Affairs.

References

Biewener, A. A. (1989). Scaling body support in mammals: Limb posture and muscle mechanics. *Science* **245**, 45–47.

Biewener, A. A. and Bertram, J. E. A. (1994). Structural response of growing bone to exercise and disuse. *J. Appl. Physiol.* **76**, 946–955.

Biewener, A. A., Fazzalari, N. L., Konieczynski, D. D. and Baudinette, R. V. (1996). Adaptive changes in trabecular architecture in relation to functional strain patterns and disuse. *Bone* **19**, 1–8.

Biewener, A. A., Thomason, J. and Lanyon, L. E. (1988). Mechanics of locomotion and jumping in the horse (*Equus*): *in vivo* stress in the tibia and metatarsus. *J. Exp. Biol.* **214**, 547–565.

Brand, R. A. (1992). Autonomous informational stability in connective tissues. *Med. Hypotheses* **37**, 107–114.

Burr, D. B. (1992). Orthopedic principles of skeletal growth, modeling and remodeling. In *Bone Biodynamics in Orthodontic*

and Orthopedic Treatment, vol. 27 (ed. D. S. Carlson and S. A. Goldstein), pp. 15–50. Ann Arbor, MI: University of Michigan.

Carter, D. R. (1984). Mechanical loading histories and cortical bone remodeling. *Calcif. Tissue Int.* **36**, S19–S24.

Carter, D. R. (1987). Mechanical loading history and skeletal biology. *J. Biomech.* **20**, 1095–1109.

Carter, D. R., Smith, D. J., Spengler, D. M., Daly, C. H. and Frankel, V. H. (1980). Measurements and analysis of *in vivo* strains on the canine radius and ulna. *J. Biomech.* **13**, 27–38.

Carter, D. R., van der Meulen, M. C. H. and Beaupre, G. S. (1996). Mechanical factors in bone growth and development. *Bone* **18** (Suppl.), 5S–10S.

Cavagna, G. A., Heglund, N. C. and Taylor, C. R. (1977). Mechanical work in terrestrial locomotion: Two basic mechanisms for minimizing energy expenditure. *Am. J. Physiol.* **233**, R243–R261.

Currey, J. D. (1984). *The Mechanical Adaptations of Bones*. Princeton, NJ: Princeton University Press. 294pp.

Currey, J. D. (1988). Strain rate and mineral content in fracture models of bone. *J. Orthop. Res.* **6**, 32–38.

Dally, J. W. and Riley, W. F. (1991). Strain-GAGE Circuits. In *Experimental Stress Analysis* (ed. L. Beamesderfer, J. Corrigan and J. M. Morriss), pp. 235–239. New York: McGraw-Hill, Inc.

Dimery, N. J. and Alexander, R. McN. (1985). Elastic properties of the hind foot of the donkey, *Equus asinus*. *J. Zool., Lond.* **207**, 9–20.

Dimery, N. J., Ker, R. F. and Alexander, R. McN. (1986). Elastic properties of the feet of deer (Cervidae). *J. Zool., Lond.* **208**, 161–169.

Evans, G. P., Behiri, J. C., Vaughan, L. C. and Bonfield, W. (1992). The response of equine cortical bone to loading at strain rates experienced *in vivo* by the galloping horse. *Equine Vet. J.* **24**, 125–128.

Frost, H. M. (1990a). Skeletal structural adaptations to mechanical usage (SATMU). I. Redefining Wolff's Law: The bone modeling problem. *Anat. Rec.* **226**, 403–413.

Frost, H. M. (1990b). Skeletal structural adaptations to mechanical usage (SATMU). II. Redefining Wolff's Law: The remodeling problem. *Anat. Rec.* **226**, 414–422.

Frost, H. M. (1997a). Defining osteopenias and osteoporoses: Another view (with insights from a new paradigm). *Bone* **20**, 385–391.

Frost, H. M. (1997b). Perspective on our age-related bone loss: Insights from a new paradigm. *J. Bone Miner. Res.* **12**, 1539–1546.

Gambaryan, P. P. (1974). Adaptation to running in the Ungulata. In *How Mammals Run*, pp. 92–162. New York: John Wiley & Sons, Inc.

Goodship, A. E., Lanyon, L. E. and McFie, H. (1979). Functional adaptation of bone to increased stress. *J. Bone Joint Surg.* **61**A, 539–546.

Hallgrimsson, B. and Swartz, S. (1995). Biomechanical adaptation of ulnar cross-sectional morphology in brachiating primates. *J. Morph.* **224**, 111–123.

Hert, J., Fiala, P. and Petrtyl, M. (1994). Osteon orientation of the diaphysis of the long bones in man. *Bone* **15**, 269–277.

Hildebrand, M. (1977). Analysis of asymmetrical gaits. *J. Mammal.* **58**, 131–156.

Huiskes, R., Weinans, H. and van Rietbergen, H. (1992). The relationship between stress shielding and bone resorption around total hip stems and the effects of flexible materials. *Clin. Orthop. Rel. Res.* **274**, 124–134.

Jayes, A. S. and Alexander, R. McN. (1978). Mechanics of locomotion of dogs (*Canis familiaris*) and sheep (*Ovis aries*). *J. Zool., Lond.* **185**, 289–308.

Judex, S., Gross, T. S., Bray, R. C. and Zernicke, R. F. (1997). Adaptation of bone to physiological stimuli. *J. Biomech.* **30**, 421–429.

Ker, R. F. (1981). Dynamic tensile properties of the plantaris tendon of sheep (*Ovis aries*). *J. Exp. Biol.* **93**, 283–302.

Lanyon, L. E. (1973). Analysis of surface bone strain in the calcaneus of sheep during normal locomotion. *J. Biomech.* **6**, 41–49.

Lanyon, L. E. (1974). Experimental support for the trajectorial theory of bone structure. *J. Bone Joint Surg.* **56**B, 160–166.

Lanyon, L. E. and Baggott, D. G. (1976). Mechanical function as an influence on the structure and form of bone. *J. Bone Joint Surg.* **58**B, 436–443.

Lanyon, L. E. and Bourn, S. (1979). The influence of mechanical function on the development and remodeling of the tibia: An experimental study in sheep. *J. Bone Joint Surg.* **61**A, 263–273.

Levenston, M. E., Beaupre, G. S., Jacobs, C. R. and Carter, D. R. (1994). The role of loading memory in bone adaptation simulations. *Bone* **15**, 177–186.

Martin, R. B. and Burr, D. B. (1989). *Structure, Function and Adaptation of Compact Bone*. New York: Raven Press. 275pp.

Martin, R. B., Mathews, S. T., Lau, S. T., Gibson, V. A. and Stover, S. M. (1996). Use of circularly *vs.* plane polarized light to quantify collagen fiber orientation in bone. *Trans. Orthop. Res. Soc.* **21**, 606.

Mason, M. W., Skedros, J. G. and Bloebaum, R. D. (1995). Evidence of strain-mode-related cortical adaptation in the diaphysis of the horse radius. *Bone* **17**, 229–237.

Mikic, B. and Carter, D. R. (1995). Bone strain gage data and theoretical models of functional adaptation. *J. Biomech.* **28**, 465–469.

O'Connor, J. A., Lanyon, L. E. and MacFie, H. (1982). The influence of strain rate on adaptive bone remodeling. *J. Biomech.* **15**, 767–781.

Pandy, M. G., Kumar, V., Berme, N. and Waldron, K. J. (1988). The dynamics of quadrupedal locomotion. *J. Biomech. Eng.* **110**, 230–237.

Pead, H. J. and Lanyon, L. E. (1990). Adaptive remodeling in bone: Torsion *versus* compression. *Trans. Orthopaed. Res. Soc.* **15**, 104.

Petrtyl, M., Hert, J. and Fiala, P. (1996). Spatial organization of the Haversian bone in man. *J. Biomech.* **29**, 161–169.

Portigliatti Barbos, M., Bianco, P., Ascenzi, A. and Boyde, A. (1984). Collagen orientation in compact bone. II. Distribution of lamellae in the whole of the human femoral shaft with reference to its mechanical properties. *Metab. Bone Dis. Rel. Res.* **5**, 309–315.

Purdue, J. R. (1983). Epiphyseal closure in white-tailed deer. *J. Wildl. Mgmnt* **47**, 1207–1213.

Reilly, G. C., Currey, J. D. and Goodship, A. E. (1997). Exercise of young thoroughbred horses increases impact strength of the third metacarpal bone. *J. Orthop. Res.* **15**, 862–868.

Riggs, C. M., Lanyon, L. E. and Boyde, A. (1993). Functional associations between collagen fibre orientation and locomotor strain direction in cortical bone of the equine radius. *Anat. Embryol.* **187**, 231–238.

Rubin, C., Gross, T., Qin, Y.-X., Fritton, S., Guilak, F. and McLeod, K. (1996). Differentiation of the bone-tissue remodeling response to axial and torsional loading in the turkey ulna. *J. Bone Joint Surg.* **78**A, 1523–1533.

Rubin, C. T. and Lanyon, L. E. (1984). Regulation of bone

formation by applied dynamic loads. *J. Bone Joint Surg.* **66**A, 397–402.

Rubin, C. T. and Lanyon, L. E. (1987). Osteoregulatory nature of mechanical stimuli: Function as a determinant for adaptive remodeling in bone. *J. Orthop. Res.* **5**, 300–310.

Rubin, C. T. and McLeod, K. J. (1996). Inhibition of osteopenia by biophysical intervention. In *Osteoporosis* (ed. R. Marcus, D. Feldman and J. Kelsey), pp. 351–371. Academic Press, New York, NY.

Skedros, J. G. (1994). Collagen fiber orientation in skeletal tension/compression systems: A potential role of variant strain stimuli in the maintenance of cortical bone organization. *J. Bone Miner. Res.* **9** (Suppl.), S251.

Skedros, J. G., Bloebaum, R. D., Mason, M. W. and Bramble, D. M. (1994a). Analysis of a tension/compression skeletal system: Possible strain-specific differences in the hierarchical organization of bone. *Anat. Rec.* **239**, 396–404.

Skedros, J. G., Chow, F. and Patzakis, M. J. (1995). The artiodactyl calcaneus as a model for examining mechanisms governing regional differences in remodeling activities in cortical bone. *J. Bone Miner. Res.* **10** (Suppl.), S441.

Skedros, J. G., Hughes, P. E. and Zirovich, M. D. (1998). Collagen fiber orientation in the turkey ulna supports a role for variant strain stimuli in cortical bone construction. *J. Bone Miner. Res.* **23** (Suppl.), S437.

Skedros, J. G., Mason, M. W. and Bloebaum, R. D. (1994b). Differences in osteonal micromorphologies between tensile and compressive cortices of a bending skeletal system: Indications of potential strain-specific differences in bone microstructure. *Anat. Rec.* **239**, 405–413.

Skedros, J. G., Mason, M. W., Nelson, M. C. and Bloebaum, R. D. (1996). Evidence of structural and material adaptation to specific strain features in cortical bone. *Anat. Rec.* **246**, 47–63.

Skedros, J. G., Su, S. C. and Bloebaum, R. D. (1997). Biomechanical implications of mineral content and microstructural variations in cortical bone of horse, elk and sheep calcanei. *Anat. Rec.* **249**, 297–316.

Skerry, T. M. and Lanyon, L. E. (1995). Interruption of disuse by short duration walking exercise does not prevent bone loss in the sheep calcaneus. *Bone* **16**, 269–274.

Skerry, T. M., Suswillo, R., El Hay, A. J., Ali, N. N., Dodds, R. A. and Lanyon, L. E. (1990). Load-induced proteoglycan orientation in bone tissue *in vivo* and *in vitro*. *Calcif. Tissue Int.* **46**, 318–326.

Takano, Y., Turner, C. H., Owan, I., Martin, R. B., Lau, S. T., Forwood, M. R. and Burr, D. B. (1999). Elastic anisotropy and collagen orientation of osteonal bone are dependent upon the mechanical strain distribution. *J. Orthop. Res.* **17**, 59–66.

Turner, C. H. (1998). Three rules for bone adaptation to mechanical stimuli. *Bone* **23**, 399–407.

Turner, C. H., Owan, I. and Takano, Y. (1995). Mechanotransduction in bone: Role of strain rate. *Am J. Physiol.* **269**, E438–E442.

van der Meulen, M. C. H., Ashford, M. W., Jr, Kiratli, B. J., Bachrach, L. K. and Carter, D. R. (1996). Determinants of femoral geometry and structure during adolescent growth. *J. Orthop. Res.* **14**, 22–29.